



A new method of processing magnesium alloy thin-walled tube by direct extrusion and corrugated equal channel angular extrusion

Zhang Ou¹ · Hu Hongjun¹ · Hu Gang¹ · Zhao Hui¹ · Ou Zhongwen²

Received: 12 October 2021 / Accepted: 7 July 2022 / Published online: 20 September 2022
© The Author(s), under exclusive licence to Springer-Verlag London Ltd., part of Springer Nature 2022

Abstract

Due to demand of strong toughness of thin-walled tube, and good secondary forming properties and high-precision dimension, new plastic-forming method should be researched to achieve a complete filling, uniform deformation, and microstructural evolution during forming process. The deformation mechanisms of a new composite extrusion for thin-walled tube fabricated by direct extrusion and corrugated equal channel angular extrusion has been researched which is shorten as “TC-ECAE” in this paper. The plastic deformation behavior of magnesium billet during TC-ECAE process was researched by DEFORMTM-3D software. Calculation parameters include material properties and process conditions have been taken into consideration. The predictions of strain distributions and damage distributions, and effective stresses distributions and flow velocities distributions have been explored. The results showed that TC-ECAE process is a magnesium alloy tube forming method suitable for industrial mass production. Serve plastic deformation of TC-ECAE would promote dynamic recrystallization which is magnesium alloy.

Keywords AZ61 magnesium alloy · Simulation · Grain refinement · Thin-walled tube · Dynamic recrystallization

1 Introduction

In the fields of automobile, electronic communication, aerospace and other fields, Magnesium alloys have become the focus of the world research. Due to its hexagonal structure magnesium alloys can be deformed difficultly at room temperature for there is few separate slip system [1, 2]. At present, the developed countries in the world have vigorously engaged in researches and development of magnesium alloy, and magnesium alloys have been widely used in the aerospace, defense industry, automobile industry, electronic devices shell, the field of sports equipment, and office supplies. Accelerations of magnesium development have become an inevitable trend.

In recent years, many new casting techniques, such as pressure casting and semi-solid casting, have been applied to the manufacture of magnesium alloys [3]. Comparing with casting process of the magnesium alloy productions, the plastic deformation can produce profiles and forging products of various sizes, the comprehensive properties of plastic formed magnesium alloy are higher than those of magnesium alloy with as cast state. So, it is very important to research and develop new types deformed magnesium alloy and new processes to manufacture wrought magnesium alloy.

As the extrusion process is a method of plastic forming, and the material are formed under three-directions compressive stress, and it is suitable for the production of low-plastic materials, so the extrusion forming is a principal technology to manufacture the forged magnesium alloy. In recent years, fine-grained structural materials processed by severe plastic deformation (SPD) have attracted increasing interest from material scientists [4]. Although it was invented in the early 1980s, this technology has not evolved as expected and is still limited to laboratory-scale experiments [5–7].

It is widely believed that extruded metal products may have uneven sizes, excellent microstructures, and favorable mechanical properties, although the extrusion speed is constant

✉ Hu Hongjun
48516686@qq.com; hhj@cqut.edu.cn

Ou Zhongwen
OuZhongwen@sina.com

¹ Materials Science and Engineering College, Chongqing University of Technology, Chongqing 400050, People's Republic of China

² School of Chemistry and Materials, Army Service College, Chongqing 401311, People's Republic of China

during extrusion [8]. The varying strains and strain rates and temperatures are critical factors of the extrusion process. In recent years, the numerical simulation of extrusion process has become a new method to prevent defects and advantageous tool to optimize the process and improve the quality of extruded products. Numerical simulations could be adopted to replace many of these experiments. The thermodynamic response of magnesium alloy under extrusion conditions is very complex. Some parameters such as stress, strain, and temperature are difficult to be measured experimentally. In this case, finite element (FE) simulation can play a unique advantage in understanding the thermal–mechanical interaction within the material during extrusion. However, there is very few study on the simulation of extrusion [9, 10].

In general, the researches on extrusion for magnesium alloy, especially make computer simulation as an auxiliary research tool has been lacking. Most of the previous studies are exploratory, the coverage is relatively narrow, process parameters do not conform to reality, or simulation method is simple, even material model is not accurate enough. Obviously, three-dimensional (3D) finite element simulation is needed to simulate thin-walled tube extrusion process, this still have high requirement on software, hardware, and user skills [11–13].

In the present research, simulation of extrusion process have been made which include direct extrusion and corrugated equal channel angular extrusion to manufacture thin walled tube, in this paper referred to as “TC-ECAE”.

The relationships between strains and stresses evolution and process conditions are lacking. It concerned characterizations of thermo-mechanical responses of wrought magnesium alloy during extrusion, that is, the evolutions of stress and strain and damage influenced by extrusion. This is much more complicated than extrusion the same billet into a tube, as result of increasing complexities in metal flow and stress distribution due to increasing contact areas and sharp edges.

To show the application potential of TC-ECAE process in industry, we designed the TC-ECAE die used in the hydropress and made simulations of TC-ECAE process. The microstructures of Mg alloy have been observed and analyzed. This study aims to clarify the grain refinement mechanisms of during TC-ECAE. In this study, the TC-ECAE process was simulated by DEFORMTM-3D finite element software, and the evolution of effective stresses, extrusion forces, and strains was obtained.

2 Simulation conditions

The description of the physical models includes the material properties of the billet, the forming temperatures, and the friction laws between the concave dies and the workpieces. Materials in simulation and extrusion experiments is wrought magnesium. The die composed of concave die,

Table 1 Physical properties of magnesium alloy

Property	Magnesium alloy
Heat transfer coefficient between tooling and billet (N/ °C s mm ²)	11
Heat transfer coefficient between tooling/billet and air(N/ °C s mm ²)	0.02
Poisson’s ratio	0.25
coefficient of linear expansion (°C ⁻¹)	2.58E – 6
Density (kg/m ³)	1780
poison’s ratio	0.45
Young’s modulus (Mpa)	47,000
Emissivity	0.12

extrusion container and extrusion rod is made of H13 die steel. The physical property of magnesium alloy is given in Table 1.

2.1 Flow stress curves for magnesium alloys

Gleeble1500D machine was used to analysis the axial compression test of hot workability. The strain rate was 0.01–10 s⁻¹ and the preheating temperature was 250 °C–500 °C. The flow stress curve under different preset strain temperatures of 250 °C, 300 °C, 350 °C, and 400 °C with strain rate of 0.01 s⁻¹ has been entered into the material property module of the DEFORMTM-3D software [12–14].

2.2 Contact and friction boundary conditions

The generalized coulomb’s law was used to explain friction behavior caused by the shear stress and the extrusion force. Shear force between workpiece and die is considered to be caused by friction [15–17] shown in Eq. (1).

$$\tau = \frac{\mu\sigma}{\sqrt{3}} \quad (1)$$

τ is shear stress, σ is equivalent stress.

2.3 Extrusion parameter between magnesium alloy and die

In this paper, the parameters in Table 2 were simulation parameters. Setting environmental temperature to 20 °C, TC-ECAE mold temperature and initial billet temperature to 400 °C. Coefficient of thermal transmission between mould and billet was 11 N/ °Cs mm², and heat transfer factor between mold/billet and atmosphere are 0.02 N/ °Cs mm² [14, 15]. The emissivity of magnesium alloy and H13 die steel is

Table 2 Simulation and experimental parameters

Extrusion speed (mm/s)	3
Friction coefficient between extrusion cylinder and billet	0.4
Friction coefficient between the billet and mold	0.4
Number of mesh divisions	20,000
Grid density type	Relative
Relative interference depth	0.7

0.12 and 0.7 respectively. The results of computer simulation were verified by TC-ECAE process experiments.

3 Numerical simulation

The longitudinal section schematic diagram of TC-ECAE die is schematically shown in Fig. 1a. The structure design of die is to match the size of the die with the blank size. The strength and the surface precision must be satisfied to obtain the surface quality of the tube. The key parts of the die container are the extrusion die, the extrusion block and

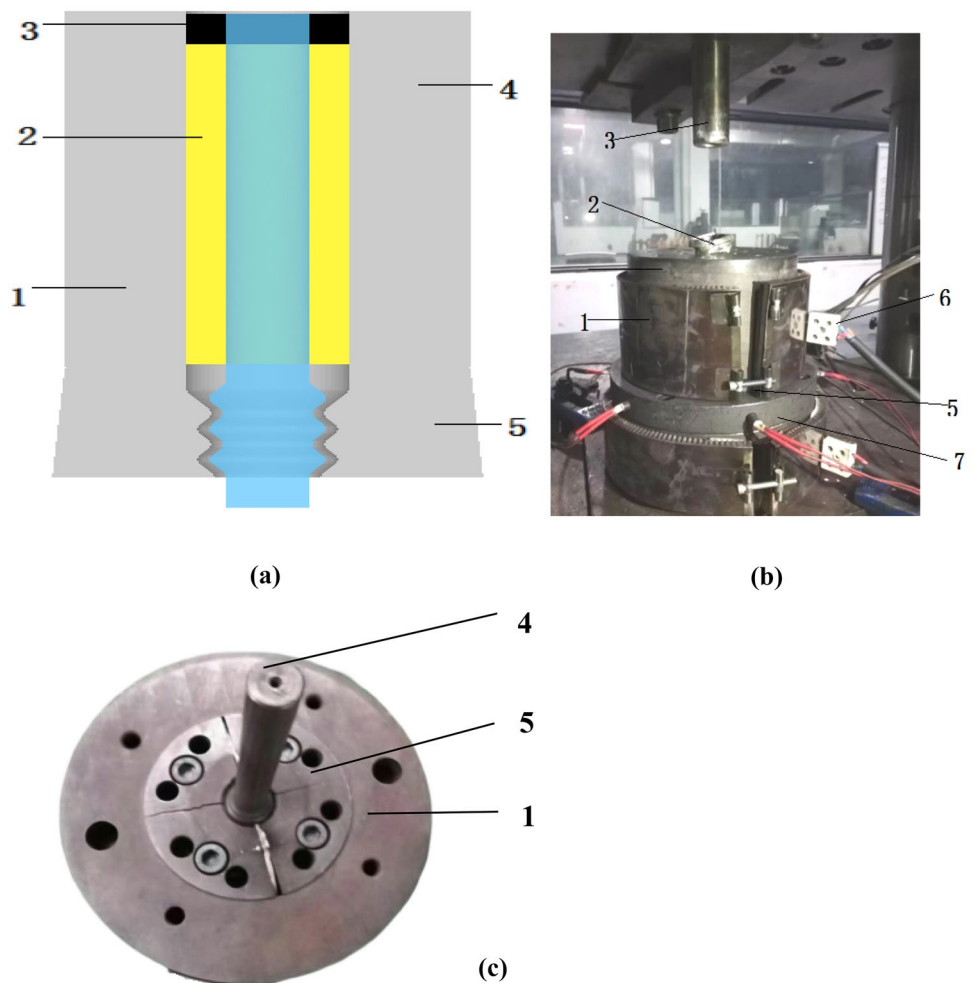
the extrusion needle, and the different extrusion ratio can be obtained by changing the different sizes of extrusion needles. The dies include direction extrusion and continuous shear structures with three section circular arcs.

4 Results and discussion

4.1 The curves of extrusion load and time

TC-ECAE process is a hot working process, the magnesium alloy may be heated over the material's recrystallization temperature to keep the material from work hardening and to make it easier to push the material through the die. The extrusion load could influent on the die life. Figure 2 illustrates that loads caused by TC-ECAE die are various during TC-ECAE process. The values for maximum forces have been obtained, and required extrusion is about 14 ton. The load curve can be divided into some stages obviously. At the initial stage of extrusion, when billet contacted with die corners, the billet began to be subjected to severe plastic

Fig. 1 (a) Three-dimensional diagram of combined concave die and billet, (b) processing device and die installation for magnesium alloy tube in the laboratory, (c) Installation between mandrel and concave die and die jackets, 1-container, 2-tube blank, 3-dummy block, 4-Fixed extrusion mandrel, 5-combined concave die, 6-heater, 7-Foundation



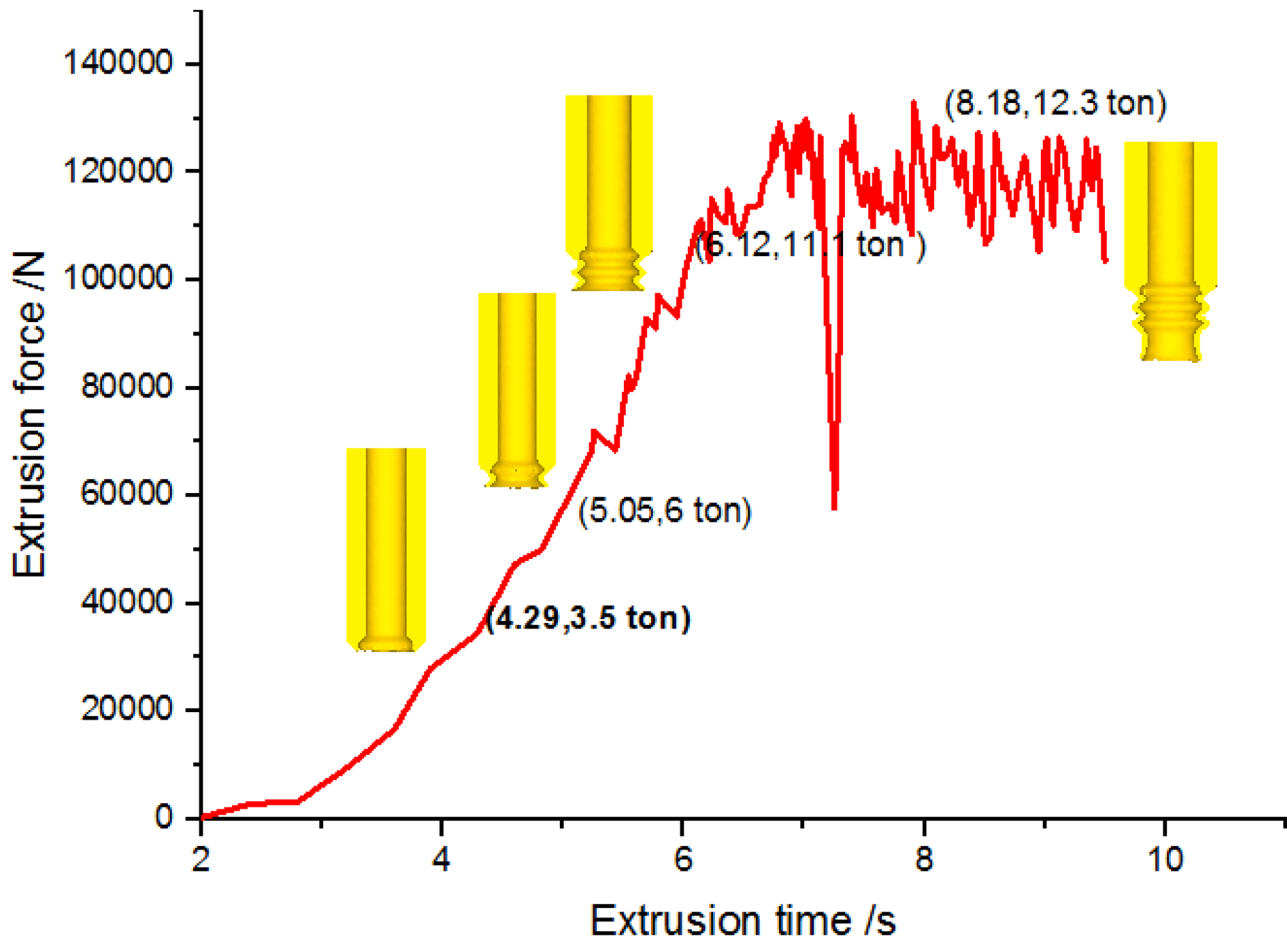


Fig. 2 The extrusion loads during TC-ECAE process

deformation, and load increased to 3.5 ton when extrusion time is 4.29 s, but this stage was not steady. The subsequent loads increased rapidly, and billet continuously passed through corrugated equal channels of the die. Further, the deformation load increased as the entire billet went through the corrugated equal channel. The deformation of billet was mainly achieved in this stage. During the third phase the average load is about 11.1 ton when extrusion time is 6.12 s. Subsequently magnesium alloy is sheared by the channels, and the maximum deformation tube load is as such as 12.3 ton. When extrusion time is about 8.18 s and the TC-ECAE process is in the steady-stage of extrusion.

4.2 Distributions of effective stress during TC-ECAE process

Examination of the predicted strains provides quantitative insight into deformation behaviors of billets during TC-ECAE process [16–18]. It is necessary to understand the

distributions and magnitudes of effective stresses during TC-ECAE process. Figure 3 shows the evolutions of effective stress contours in magnesium billet during different TC-ECAE, which provide the important information of stress distribution. Figure 3a, b, c and d are the distributions of the equivalent stress for extrusion time 4.29 s, 5.05 s, 6.12 s and 8.18 s respectively. The effective stresses of the material are not even which are seen from the Fig. 3, and the maximum effective stress is about 36.3 MPa at extrusion time 4.29 s. The deformation of the initial extrusion is nonuniform, and the highest stress (36 MPa) located at outer corner when extrusion time is 5.05 s. Distributions of the stress are lamellar with distinct deformation gradients. The deformation is close to the simple shear deformation, but the stress focus on deformation zone in the extrusion time 8.18 s. The maximum stress increase to 320 MPa. From the stress evolution during the TC-ECAE process it can be found stress decrease with the TC-ECAE progressing, the reason is that the dynamic recrystallization has taken place.

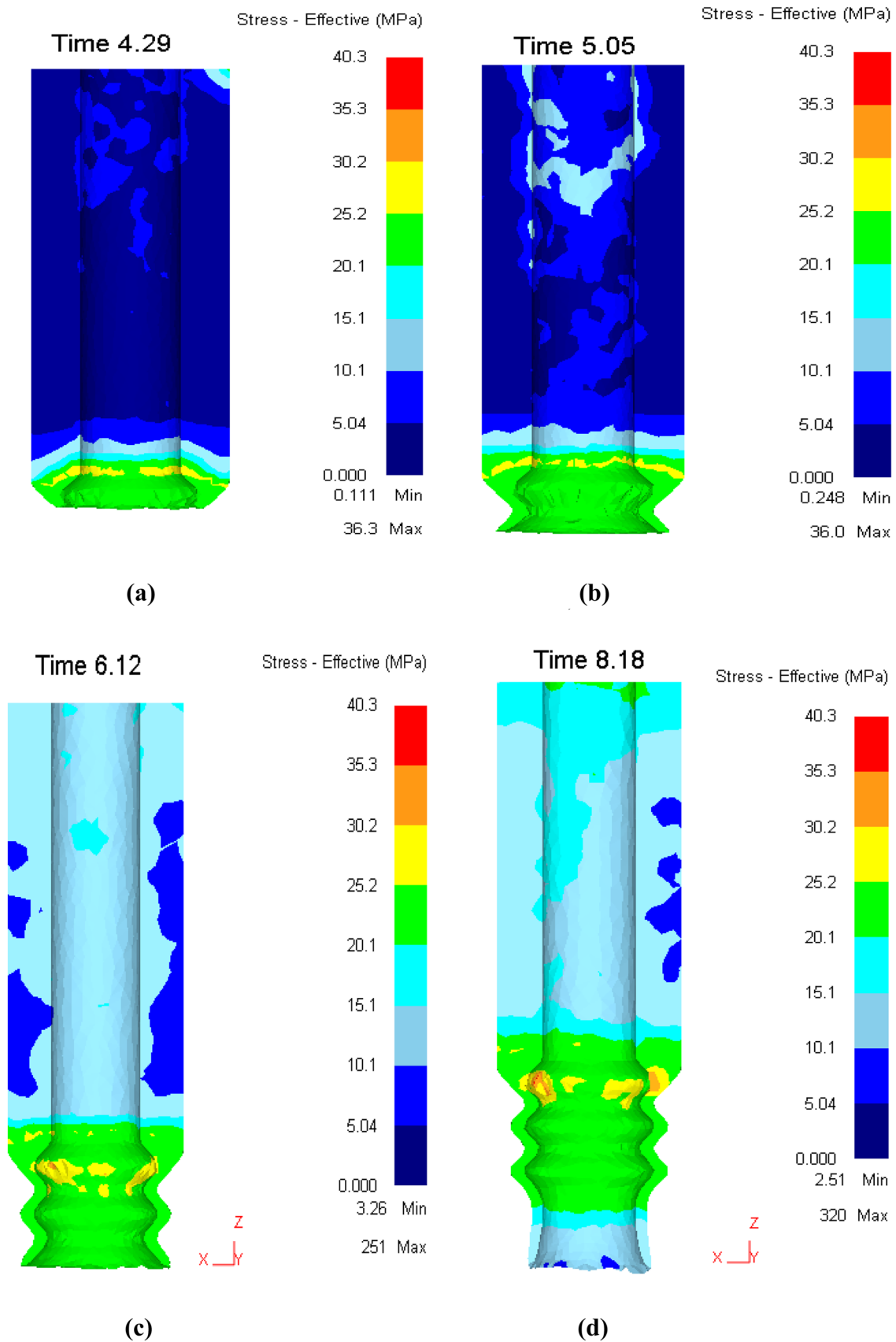


Fig. 3 Evolutions of effective stress contours in billet during different periods for TC-ECAE process, (a) 4.29 s, (b) 5.05 s, (c) 6.12 s and (d) 8.18 s

4.3 Analysis of flow velocities

Vector plots display magnitude and direction. Magnitude is indicated by vector length and color. Contour plots display only magnitude, where contour color indicates TC-ECAE velocity magnitude. Figure 4 shows velocity field of metal flow during TC-ECAE process. An approximate sector with severe deformation in Fig. 6a and a dead metal zone exists near the export parts of die. Some metal moves perpendicular to the interface of the bottom die, while the other moves toward the container, and the dead zone are formed. Figure 4a shows the dead metal zone where the material flow velocity is smaller than 7.5 mm/s, represented by the wathet blue area at the corners between the container liner and die face. The flow discontinuity at the boundary between the deformation zone and dead metal zone is clearly revealed which is area of inactive metal that generally remains dormant and stagnant throughout the extrusion process. It is the shearing at this boundary which leads to the formation of extrusion surface from the virgin material in the interior of the billet. It was profitable that the dead metal zone kept the oxidated layer on the surface of billet staying in the container, and which prevent oxidated layer from entering the inner of workpiece.

While the front of flowing metal arrived at the lower underside of the die, a small static zone in Fig. 4b was formed when the direct extrusion stage was over. In the Fig. 4c and d the metal near the container flows towards the bottom die homogeneously, and less velocity vector toward the interfaces is observed in the plastic deformation zone, and the metal flows toward TC-ECAE die without large angle turning, which not only decreases the generation of flow lines turbulence, dead zone and overlaps, but also improves the extruded product quality.

4.4 Damage prediction

Damage has been shown to be a good indicator of certain types of tensile ductile fracture. Workability is usually thought as being limited by the onset of the fracture. Greater workability of the material allows greater deformation. In this study many types of ductile fracture criteria were used to determine the limit of the bulk deformation. The empirical formulas of these criteria are described below. The modeling formulations of various ductility damage values are presented in Ref. [19, 20]. The present study considers the following damage values in Eq. (2) [21–23].

$$\int_0^{\bar{\epsilon}_f} \frac{\sigma_{\max}}{\bar{\sigma}} d\bar{\epsilon} = C \quad (2)$$

where $\bar{\sigma}_{\max}$ is the maximum ductility stress; σ_1 and σ_2 are the principal stresses; $\bar{\sigma}$ is the effective stress; $\bar{\epsilon}$ is the effective

strain; σ_m is the hydraulic compressive stress (mean stress); n the strain hardening exponent; $\bar{\epsilon}_f$ the effective strain of fracture; F is a material deformation function; C is the damage value of the material. In order to calculate ductile fracture criteria, destructive tests had been done and Compression tests have been carried out. Cockcroft and Latham predicted that fracture occurs in a ductile material at a critical damage factor value C^* of the damage factor C . The C-L criterion for ductile fracture during metalworking was applied in conjunction with fracture strains measured from uniaxial tension tests. In uniaxial tension tests, in which sharp necks and high levels of stress triaxiality are negligible. The fracture strain $\bar{\epsilon}_f$ derived from the magnesium alloy stress/strain curve is approximately 0.45. Thus, the value of C^* is 0.45.

The experimental results showed that the fracture model adapted in these simulations was Cockcroft and Latham fracture model in Eq. (2) whose value was set to 0.45. Figure 5 represents the damage inclination indexes at extrusion time 4.29 s, 5.05 s, 6.12 s and 8.18 s, respectively. It can be seen that the index of the damage at extrusion time 5.05 s is as much as 0.908. And at the extrusion time 8.18 the index is about 0.817. It is seen that the maximum damage occurs at the billet surface in the exit region of the die for direct extrusion. The reason could be attributed to the critical damage at the point of maximum tensile stress in the tube.

4.5 Microstructural evolutions during TC-ECAE process

Grain sizes evolutions of four parts in rod formed by TC-ECAE process are shown in Fig. 6. The microstructures with as cast state with average grain size 200 μm are shown in (a), which indicates that the deformation degree is very small. As the deformation continues, the width of rod-like microstructures with average grain size 150 μm may become narrow, a number of lamellar-structure twins may appear in the grains shown in (b), because dynamic crystallization would taken place. The uniform deformation have taken place in the grains mainly and improved the formation of rod-like microstructures while recrystallization may occur in a small number of grains. Rod-like and lamellar microstructures fabricated by direct extrusion began to reduce for the large shear strains caused by shear deformation in this zone and the deformation grains with average grain size 100 μm would turn into dynamic recrystallization grains shown in (c). In the shearing zones, dynamic recrystallization may happen sufficiently for five shearings with average grain size 40 μm shown in (d). Use of TC-ECAE process, the average grain size may be refined effectively. Microstructures are not only clearly refined but also relatively uniform. This is because the TC-ECAE process include additional five shearings and which is more than direct extrusion. So the deformation degree of central part of rods increased, part recrystallization

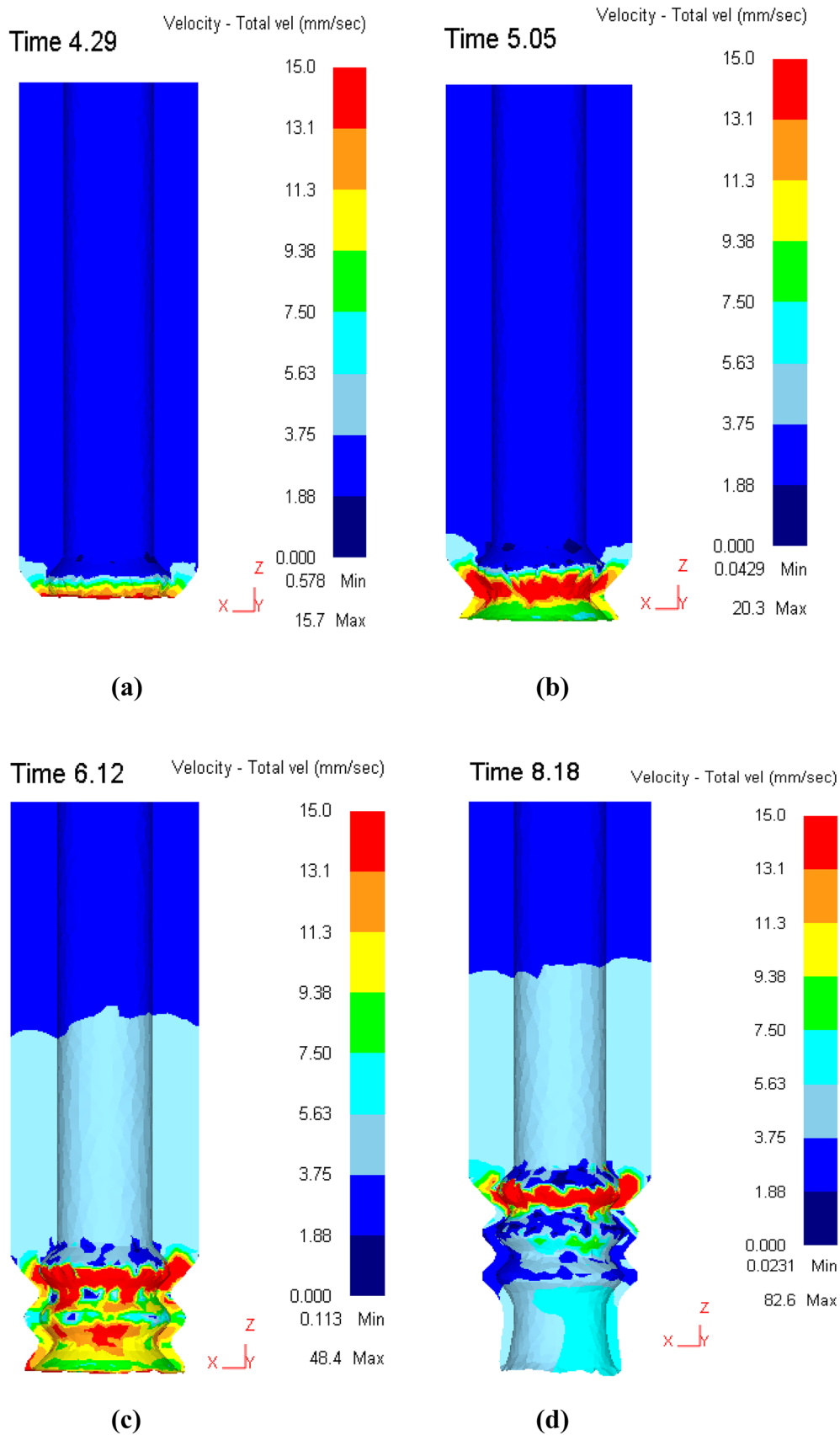


Fig. 4 The flow velocity fields during TC-ECAE process, **(a)** 4.29 s, **(b)** 5.05 s, **(c)** 6.12 s and **(d)** 8.18 s

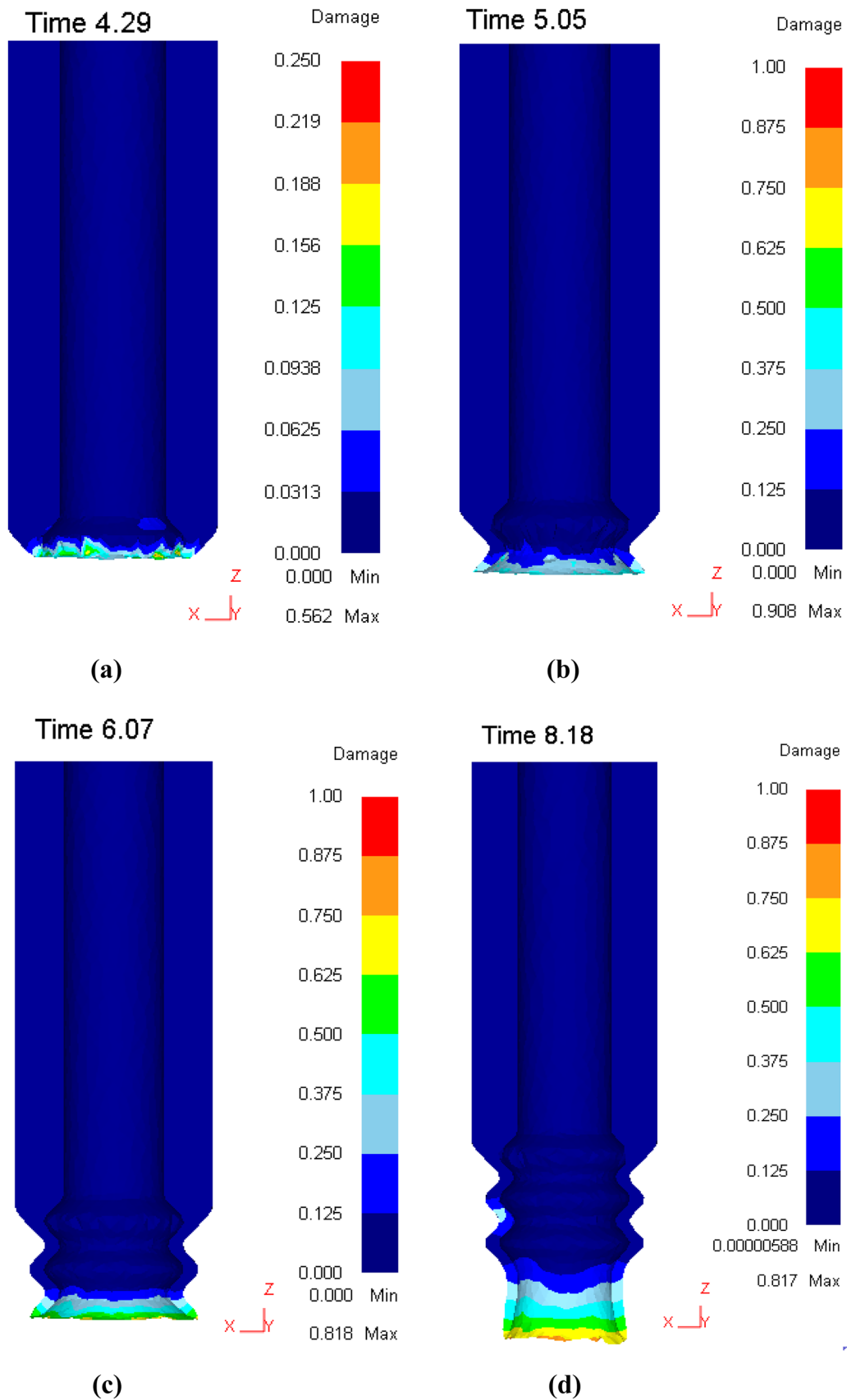
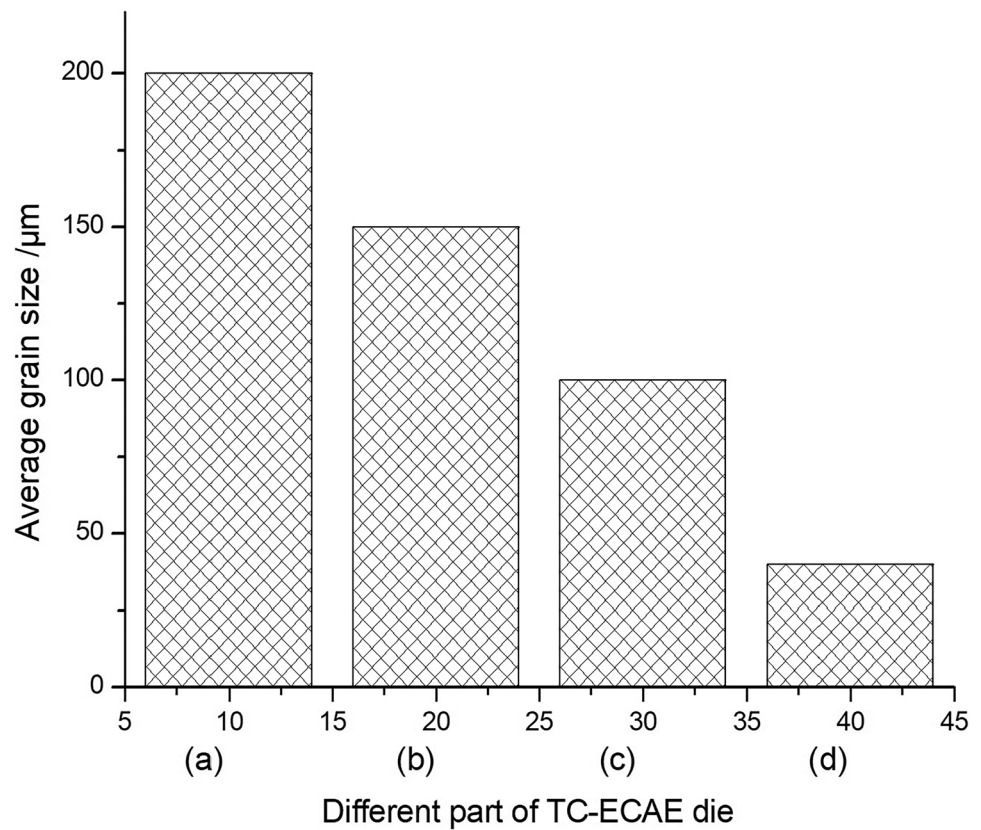


Fig. 5 Crack initiation predicted by normalized Crockcroft and Latham fracture model, (a) 4.29 s, (b) 5.05 s, (c) 6.12 s and (d) 8.18 s

Fig. 6 Microstructures of magnesium alloy in different part of TC-ECAE die, (a) 4.29 s, (b) 5.05 s, (c) 6.12 s and (d) 8.18 s



occurred. Therefore, the microstructures became smaller and more homogeneous.

The relationship between the average recrystallization grain size (d) and the Zener-Hollomon parameter (Z) during dynamic recrystallization is given by $-\ln d = A + B \ln Z$. Based on the present TC-ECAE process, average accumulative strains, strain rates and Z parameters of the magnesium alloy increase with the development of TC-ECAE process [24–26]. It can be found that accumulative strains increase with the advance of TC-ECAE process, so the grains would be refined consequently. It is clear that there are three steps recrystallization during TC-ECAE process. It can be found that the average sizes of grains for DRX were coarsened with the preheated temperature increasing [23, 27–29].

5 Conclusions

This study has utilized three-dimensional finite element DEFORM software to research the plastic deformation behavior of magnesium billet during TC-ECAE process through a TC-ECAE combination die. The research results have been shown as follows:

- (1) The extrusion load curve can be divided into four stages including the extrusion upsetting stage and the direction extrusion stage and multi-shearings obtained from

simulation results. The evolutions of extrusion load curves and effective stresses and temperatures can be divided into four stages.

- (2) The maximum damage occurs on the billet surface in the exit region owing to maximum tensile stress.
- (3) The TC-ECAE process would cause severe plastic deformation and improve the dynamic recrystallization during TC-ECAE process, and TC-ECAE is an efficient and inexpensive grain refinement method for magnesium alloys.
- (4) The large strains can be introduced into the extrusion and continuous multi-shearings deformation, which promote the occurrence of dynamic recrystallization of magnesium alloys.

Acknowledgements This work was supported by Chongqing Natural Science Foundation Project of cstc2018jcyjAX0653.

Authors' contributions Zhang Ou done the experiments in this paper. Hu Hongjun is the corresponding author of this paper who wrote the paper. Hu Gang done the simulation in this paper. Zhao Hui done the testings in this paper. Ou Zhongwen the second corresponding author in this paper.

Data availability The raw/processed data required to reproduce these findings cannot be shared at this time as the data also forms part of an ongoing study.

Declarations

Ethical approval No animals have been used in any experiments.

Consent to participate There are no human who have been used in any experiments.

Consent for publication The authors confirm that the work described has not been published before (except in the form of an abstract or as part of a published lecture, review, or thesis); that it is not under consideration for publication elsewhere; that its publication has been approved by all co-authors, if any; and that its publication has been approved (tacitly or explicitly) by the responsible authorities at the institution where the work is carried out. The authors agree to publication in the journal indicated below and also to publication of the article in English by Springer in Springer's corresponding English-language journal.

Disclaimer The copyright to the English-language article is transferred to Springer effective if and when the article is accepted for publication. The author warrants that his/her contribution is original and that he/she has full power to make this grant. The author signs for and accepts responsibility for releasing this material on behalf of any and all co-authors. The copyright transfer covers the exclusive right to reproduce and distribute the article, including reprints, translations, photographic reproductions, microform, electronic form (offline, online) or any other reproductions of similar nature. After submission of the agreement signed by the corresponding author, changes of authorship or in the order of the authors listed will not be accepted by Springer.

Competing interests The authors declare that they have no competing interests.

References

- Han D, Zhang J, Huang J, Yong L, He G (2020) A review on ignition mechanisms and characteristics of magnesium alloys. *J Magnes Alloys* 2:329–344. <https://doi.org/10.1016/j.jma.2019.11.014>
- Giuliano G, Polini W (2021) Optimal design of blank thickness in superplastic AZ31 alloy to decrease forming time and product weight. *Int J Adv Manuf Technol*. <https://doi.org/10.1007/s00170-021-08062-7>
- Xu Y, Ke L, Ouyang S, Mao Y, Niu P (2021) Precipitation behavior of intermetallic compounds and their effect on mechanical properties of thick plate friction stir welded Al/Mg joint. *J Manuf Process* 64:1059–1069. <https://doi.org/10.1016/j.jmapro.2020.12.068>
- Kumar SD, Kumar SS (2021) Effect of heat treatment conditions on ballistic behaviour of various zones of friction stir welded magnesium alloy joints. *Trans Nonferrous Met Soc China* (1). [https://doi.org/10.1016/S1003-6326\(20\)65484-X](https://doi.org/10.1016/S1003-6326(20)65484-X)
- Yuan S, Xia Q, Long J, Xiao G, Cheng X (2020) Study of the microstructures and mechanical properties of ZK61 magnesium alloy cylindrical parts with inner ribs formed by hot power spinning. *Int J Adv Manuf Technol* 111:851–860. <https://doi.org/10.1007/s00170-020-06091-2>
- Huang J, Song G, Zhu Y, Zheng, D, Wang Z (2021) The anodically polarized Mg surface products and accelerated hydrogen evolution. *J Magnes Alloys*(7). <https://doi.org/10.1016/j.jma.2021.05.008>
- Ji Y, Duan J, Li H, Liu Y, Peng W, Ma L (2021) Improvement of edge crack damage of magnesium alloy by optimizing the edge curve during cross variable thickness rolling. *Int J Adv Manuf Technol* 112:1993–2002. <https://doi.org/10.1007/s00170-020-06517-x>
- Siahsarani A, Faraji G (2021) Processing and characterization of AZ91 magnesium alloys via a novel severe plastic deformation method: Hydrostatic cyclic extrusion compression (HCEC). *Trans Nonferrous Met Soc China* (5). [https://doi.org/10.1016/S1003-6326\(21\)65579-6](https://doi.org/10.1016/S1003-6326(21)65579-6)
- Cai S, Li Q (2021) Analysis of the forming behaviors of magnesium alloy AZ31 by vaporizing metal foils. *Int J Adv Manuf Technol* 114:929–937. <https://doi.org/10.1007/s00170-021-06970-2>
- Tian Y, Hu H, Liang P, Zhang D, Ou Z (2021) Influences of expanding angles on extrusion-shearing-expanding processing of AZ31 magnesium alloy thin-walled tubes. *Int J Adv Manuf Technol*. <https://doi.org/10.1007/s00170-021-07898-3>
- Chen Q, Zhang X, Lin J, Zhan H, Zhao Z, Xie Z, Yuan B (2019) Isothermal closed-die forming process of magnesium alloy upper receiver: numerical simulation and experiments. *Int J Adv Manuf Technol* 102:685–694. <https://doi.org/10.1007/s00170-018-03209-5>
- Li X, Li F, Li X (2018) Effect of different temperatures on deformation characteristics of AZ31 magnesium alloy by continuous variable cross-section direct extrusion. *Int J Adv Manuf Technol* 95:4623–4628. <https://doi.org/10.1007/s00170-017-1557-6>
- Yang X, Feng W, Li W, Yao S (2019) Microstructure and properties of probeless friction stir spot welding of AZ31 magnesium alloy joints. *Trans Nonferrous Met Soc China* (11). [https://doi.org/10.1016/S1003-6326\(19\)65136-8](https://doi.org/10.1016/S1003-6326(19)65136-8)
- Ahmadi S, Alimirzaloo V, Faraji G, Doniavi A (2021) Properties inhomogeneity of AM60 magnesium alloy processed by cyclic extrusion compression angular pressing followed by extrusion. *Trans Nonferrous Met Soc China* 21(3):65527–65529. [https://doi.org/10.1016/S1003-6326\(21\)65527-9](https://doi.org/10.1016/S1003-6326(21)65527-9)
- Ding Y, Wang J, Zhao M, Ju D (2018) Effect of annealing temperature on joints of diffusion bonded Mg/Al alloy. *Trans Nonferrous Met Soc China* 28(2):251–258. [https://doi.org/10.1016/S1003-6326\(18\)64658-8](https://doi.org/10.1016/S1003-6326(18)64658-8)
- Hu H, Hong X, Tian Y, Zhang D (2021) AZ31 magnesium alloy tube manufactured by composite forming technology including extruded-shear and bending based on finite element numerical simulation and experiments. *Int J Adv Manuf Technol* 115:2395–2402. <https://doi.org/10.1007/s00170-021-07242-9>
- Campanella D, Buffa G, Lo Valvo E, Fratini L (2021) A numerical approach for the modelling of forming limits in hot incremental forming of AZ31 magnesium alloy. *Int J Adv Manuf Technol* 114:3229–3239. <https://doi.org/10.1007/s00170-021-07059-6>
- Li X, Jiang J, Zhao Y, Ma A, Wen D, Zhu Y (2015) Effect of equal-channel angular pressing and aging on corrosion behavior of ZK60 Mg alloy. *Trans Nonferrous Met Soc China* 25(12):3909–3920. [https://doi.org/10.1016/S1003-6326\(15\)64038-9](https://doi.org/10.1016/S1003-6326(15)64038-9)
- Önder A (2019) A forming load analysis for extrusion process of AZ31 magnesium. *Trans Nonferrous Met Soc China* 29(4):741–753. [https://doi.org/10.1016/S1003-6326\(19\)64984-8](https://doi.org/10.1016/S1003-6326(19)64984-8)
- Xia Y, Wu L, Yao W, Hao M, Chen J, Zhang C, Pan F (2021) In-situ layered double hydroxides on Mg–Ca alloy: Role of calcium in magnesium alloy. *Trans Nonferrous Met Soc China* 31(6):1612–1627. [https://doi.org/10.1016/S1003-6326\(21\)65527-9](https://doi.org/10.1016/S1003-6326(21)65527-9)
- Wang B, Wang F, Wang Z, Liu Z, Mao P (2021) Fabrication of fine-grained, high strength and toughness Mg alloy by extrusion-shearing process. *Trans. Nonferrous Met Soc China* 31(3):666–678. [https://doi.org/10.1016/S1003-6326\(21\)65528-0](https://doi.org/10.1016/S1003-6326(21)65528-0)
- Siahsarani A, Faraji G (2021) Processing and characterization of AZ91 magnesium alloys via a novel severe plastic deformation method: Hydrostatic cyclic extrusion compression (HCEC). *Trans Nonferrous Met Soc China* 31(5):1303–1321. [https://doi.org/10.1016/S1003-6326\(21\)65579-6](https://doi.org/10.1016/S1003-6326(21)65579-6)

23. Liu D, Liu Z, Wang E (2015) Evolution of twins and texture and its effects on mechanical properties of AZ31 magnesium alloy sheets under different rolling process parameters. *Trans Nonferrous Met Soc China* 25(11):3585–3594
24. Guo L, Fu F (2018) Effect of deformation mode, dynamic recrystallization and twinning on rolling texture evolution of AZ31 magnesium alloy. *Trans Nonferrous Met Soc China* 28:1094–1102. [https://doi.org/10.1016/S1003-6326\(18\)64745-4](https://doi.org/10.1016/S1003-6326(18)64745-4)
25. Mehra D, Mahapatra M, Harsha S, Magnes J (2018) Processing of insitu RZ5–10wt%TiC magnesium matrix composite *J Magnes and Alloy* 6:100–105. <https://doi.org/10.1016/j.jma.2018.01.002>
26. Huang H, Liu H, Wang C, Sun J, Bai J, Xue F, Jiang J, Ma A (2019) Potential of multi-pass ECAP on improving the mechanical properties of a high-calcium-content Mg-Al-Ca-Mn alloy. *J Magnes Alloys* 7:617–627. <https://doi.org/10.1016/j.jma.2019.04.008>
27. Sheng K, Lu L, Xiang Y, Ma M, Wu Z (2019) Crack behavior in Mg/Al alloy thin sheet during hot compound extrusion. *J Magnes Alloys* 7:717–724. <https://doi.org/10.1016/j.jma.2019.09.006>
28. Du Y, Liu D, Ge Y, Jiang B (2020) Effects of deformation parameters on microstructure and texture of Mg-Zn-Ce alloy. *Trans Nonferrous Met Soc China* 30:2658–2668. [https://doi.org/10.1016/S1003-6326\(20\)65410-3](https://doi.org/10.1016/S1003-6326(20)65410-3)
29. Guo F, Zhang D, Yang X (2015) Microstructure and texture evolution of AZ31 magnesium alloy during large strain hot rolling. *Trans Nonferrous Met Soc China* 25(01):14–21. [https://doi.org/10.1016/S1003-6326\(15\)63573-7](https://doi.org/10.1016/S1003-6326(15)63573-7)

Publisher's Note Springer Nature remains neutral with regard to jurisdictional claims in published maps and institutional affiliations.

Springer Nature or its licensor holds exclusive rights to this article under a publishing agreement with the author(s) or other rightsholder(s); author self-archiving of the accepted manuscript version of this article is solely governed by the terms of such publishing agreement and applicable law.